energies

MDPI

Article

Inverse Design of Axis Fan for Permanent Magnet Drive Motor for Special Vehicles

Changjun Ma [1], Chunming Li [2], Kai Liu [1], Zhixiang He [3], Daqian Pang [2] and Wei Hua [1,*]

1 School of Electrical Engineering, Southeast University, Nanjing 210096, China; 15810189657@163.com (C.M.); kliu@seu.edu.cn (K.L.)
2 China North Vehicle Research Institute, Beijing 100072, China; chunming@noveri.com.cn (C.L.); pangdaqian@sina.com (D.P.)
3 College of Electrical and Information Engineering, Hunan University, Changsha 410000, China; hzx0920@hnu.edu.cn
* Correspondence: huawei1978@seu.edu.cn

Abstract: The control of mechanical energy loss is especially key in the design of permanent magnet drive motors for special vehicles. This paper takes a 300 kW high-efficiency motor as an example, and under the operating condition of 9000 rev/min, in order to control the size of the mechanical loss P_{mech}, improve the efficiency of the motor, as well as enhance the ventilation and heat dissipation performance of the motor, the structural parameters of the motor's Axis fan are identified by using the Reverse Engineering (RE), and the fan performance is simulated and analysed by using the standard k-ε turbulence model of Computational Fluid Dynamics. The mechanical loss calculation model is investigated, and the effects of different blade numbers, wrap angles, and mounting angle parameters of the fan on the mechanical loss P_{mech} are derived. And finally, the scheme is calculated to show that when the blade number Z is 13, the wrap angle $\Delta\varphi$ is 60°, the front mounting angle Φ_1 is 45°, and the rear mounting angle Φ_2 is 30°, the mechanical loss P_{mech} decreases from 8.0 kW to 2.54 kW, and the motor efficiency η_0 is greatly improved, increasing from 94.2% to 96.1%. Meanwhile, based on finite element simulation experiments, the effects of the motor Axis fan on the steady-state temperature field of the pre-optimised and post-optimised fans are compared, and the optimised axis fan makes the motor ventilation and heat dissipation more reasonable. The maximum temperature of the motor under the same working condition decreased by 16.7 K, the efficiency η_0 of this motor was greatly improved, and the efficiency η_0 increased from 94.2% to 96.1%.

Keywords: high-efficiency motor; mechanical loss; axis fan; temperature field; turbulence model

check for updates

Citation: Ma, C.; Li, C.; Liu, K.; He, Z.; Pang, D.; Hua, W. Inverse Design of Axis Fan for Permanent Magnet Drive Motor for Special Vehicles. *Energies* **2023**, *16*, 7685. https://doi.org/10.3390/en16237685

Academic Editor: Mario Marchesoni

Received: 24 October 2023
Revised: 10 November 2023
Accepted: 15 November 2023
Published: 21 November 2023

1. Introduction

Permanent magnet synchronous drive motors for special vehicles play a pivotal role in national modernisation and defence construction. Permanent magnet synchronous motors (PMSMs), with their high efficiency and small size, have become one of the key components of electric drive systems in special vehicles [1–5]. Such drive motors have an extremely high power density, reaching more than four times the power density of general industrial motors. Special vehicles have small spaces, heat dissipation difficulties, and motor operations at high ambient temperatures. At the same time, the special performance requirements of special vehicles include acceleration, deceleration, high torque, low speed, high speed, constant power, and other states between frequent conversions [6]. Easily caused by the permanent magnet synchronous motor loss increase, motor components local overheating, resulting in the winding and permanent magnets, there are serious safety hazards [7]. This poses a great challenge to the temperature rise of the motor. The temperature rise of the motor is not only an important index to measure the performance of the motor but also the temperature of the permanent magnets, which determines its anti-demagnetisation capability. Therefore, in the design of permanent magnet motors for special vehicles, it is of great significance to comprehensively analyse the temperature field of the motor and a detailed thermal management design is required [8–11].

Conventional motor development studies generally calculate the temperature rise of the windings and magnets of the motor. Literature [12] studied the electromagnetic design of a 350 kW permanent magnet propulsion motor for tanks. The losses of the motor are analysed and calculated, and the steady-state temperature rise of the motor is calculated by the finite element method. In [3], a three-dimensional fluid-solid coupling simulation model of the motor was established, and a hybrid ventilation and heat dissipation system was proposed. In [13], the effects of different cooling methods on the motor are investigated, and the advantages and disadvantages of various cooling methods are compared. Ref. [14], for hybrid electric vehicle motors, the performance of the air-water hybrid cooling system is investigated, and a reduced-order thermal model is used to predict the internal temperature of the motor. This literature mainly conducted relevant research on two methods of motor ventilation and heat dissipation, namely air cooling and water cooling. The impact of motor fan structure on motor temperature rise performance has not been addressed.

The axis fan of the permanent magnet drive motor for special vehicles is a very important ventilation and heat dissipation component in the drive motor. The performance of the fan directly affects the size of the mechanical loss of the motor as well as the heat dissipation ability of the motor, thus affecting the performance and service life of the motor. In [15], a thermofluid analysis of the air cooling of a permanent magnet motor with a shaft fan was carried out, but the thermal performance of each component of the motor was not analysed in detail. Ref. [16], the effect of an auxiliary cooling fan on the ventilation and heat dissipation of the motor was studied, and a more accurate thermal model of the motor was developed. Ref. [17], the method of internal and external aerodynamic analysis based on computational fluid dynamics (CFD) was used to analyse and calculate the internal mechanical losses of the motor. In Refs. [18–21], theoretical and numerical analyses as well as motor temperature field studies have been carried out for shaft fans (axial fans) or forced fans of electric motors. The above literature has studied the thermal field calculation method and structural design of motor ventilation and cooling systems, especially the new motor ventilation and cooling system. But the problem is that there is no accurate calculation model for the mechanical loss of the motor fan. The control of the mechanical energy loss of the motor fan is not addressed. The reduction of mechanical energy losses in the fan reduces the temperature rise of the motor, which in turn improves the overall performance of the motor.

Reverse Engineering (RE), also known as inverse design, refers to the measurement of existing models or parts to get the required data and importing the measurement data into 3D software (ANSYS-CFturbo 2022) to get a complete CAD model. On this basis, the model can be improved and optimised more easily by analysing the designer's design intention and adding new ideas [22]. RE inverse engineering can be used to optimize the design of the cooling fan, optimize and innovate the fan structure, save R&D costs, and shorten the R&D cycle. In Refs. [23–25], the key aspects of data measurement, data analysis and processing, and surface reconstruction in the reverse engineering of ventilation cooling fans are studied, and the characteristics of curves/surfaces such as Bezier, B-Spline, and NURBS are compared and analysed. The finite element analysis method is used to simulate and analyse the internal flow field, structure, and modal state of the fan. Ref. [22], the surface of the motor fan is reconstructed using inverse engineering, and the flow characteristics of the inverse fan model are analysed using hydrodynamics and verified experimentally, which fails to make a detailed study on the thermal performance of the motor fan and the efficiency of the motor.

None of the above studies have dealt with the reverse design (RE) of the axis fan of special vehicle drive motors, in particular. There are very few studies on the effect of fan structure parameters on motor fan performance and mechanical energy loss, and too few studies on the effect of fan optimisation on the motor ventilation and cooling system as well as on the efficiency of the motor.

With the increasingly high requirements for motor efficiency, how to be able to further control to reduce the mechanical loss of the motor has become the focus of research. The cooling fan of the motor plays an important role in the mechanical loss, vibration, noise, and temperature rise of the motor. The design of a new type of motor fan in line with fluid flow characteristics to meet the needs of the development of high-efficiency, ultra-high-efficiency motors is a very meaningful work [26].

The object of this paper is the axis cooling fan for permanent magnet drive motors for special vehicles. A new way of thinking is proposed to study the influence of motor fan structure on the temperature rise performance of the motor, especially on the calculation of the mechanical energy loss of the motor fan, to establish a more accurate finite element calculation model. Reduced motor temperature rise by reducing mechanical energy losses. Then it improves the overall performance of the motor. The structural parameters of the fan are identified by using the inverse solving technique. And the fan structure parameters are improved and optimised, and the effects of different fan structure parameters on mechanical energy loss are analysed. The fan structure is optimised and an accurate mechanical loss calculation model is established. At the same time, the mechanical loss of the motor was reduced. And reduced motor temperature rise, which in turn improved the overall motor efficiency. Finally, finite element simulation experiments were carried out on the motor to compare the effects of the fan before and after optimisation on the steady-state maximum temperature T_{max} and maximum temperature rise ΔT of the motor.

2. Motor Axis Fan Model and Basic Theory

2.1. Motor Overall Structure and Cooling Fan Model

The motor adopts an air-water composite cooling structure, and its motor structure and cooling circuit are shown in Figure 1. The motor mainly consists of stator and rotor cores, windings, permanent magnets, rotor shafts, chassis, waterways, axis fan (rotor shaft fan), air-cooling device, and other components. The motor adopts the composite cooling method of water cooling in the spiral water channel of the casing and the cooling fan of the rotor shaft to disturb the internal air circulation. The motor base is equipped with a spiral water jacket. The cooling water flows into the motor from the inlet of the water channel, then flows along the axial spiral, and finally flows out of the outlet of the water channel to take away the heat to cool the motor. At the same time, the motor uses a rotor cooling fan to disturb the internal air cooling. The air passes through the rotor vent into the fan side of the end cavity, the side of the end cavity of the air part of the air gap, and the other part of the water-cooled device through the seat after the collection of the other side of the end cavity into the rotor vent, forming a circular loop. The red arrow shows the water cooling circuit, and the green arrow shows the internal air circulation cooling circuit.

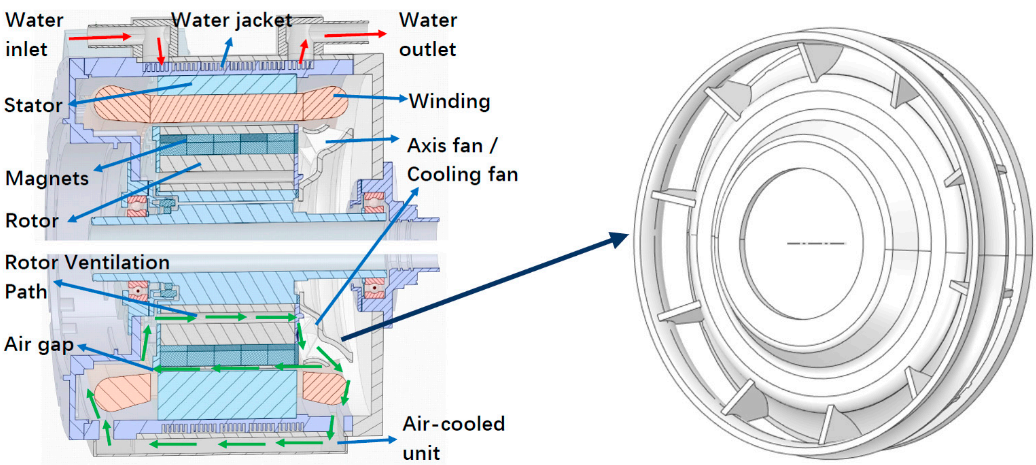

Figure 1. Motor structure and cooling fan.

2.2. Calculation of Mechanical Energy Loss in Electric Motors

As shown in Equation (1), the total power P of the motor in this paper is 300 kW, and the efficiency η_0 is 94.2%. In addition to the external active power output P_1 of the motor, the various energy losses are copper consumption P_{cu}, iron consumption P_{fe}, magnetic steel eddy current consumption P_{mag}, mechanical loss P_{mech}, and stray loss P_σ [27]. Among them, the mechanical energy loss P_{mech} is 8 kW. And the objective of this study is to control the mechanical energy loss below 4 kW so that the efficiency of the motor can be increased to more than 95.5%.

$$P = P_1 + P_{cu} + P_{fe} + P_{mag} + P_{mech} + P_\sigma$$

$$\eta_0 = \frac{P_1}{P} \tag{1}$$

During the high-speed rotation of the motor, the fan, as well as the rotor, generate mechanical energy losses P_{mech}. The total motor fan torque magnitude can be obtained by using the CFD post-processing function [28]. Equation (2) is then used to evaluate the power loss P_{mech} of the fan component.

$$P_{mech} = M\omega \tag{2}$$

where M is the total fan torque magnitude in Nm; ω is the rotor angular velocity in 1/s.

3. Basic Theory of Fan Blades

3.1. Calculation of Fan Blades and Flow Rate Based on Empirical Equations

The impeller is the most important part of the ventilator fan, and the basic methods commonly used are introduced here. Fan blade size can be determined according to the size of the motor fan installation space, and the main dimensions of the fan impeller, as shown in Figure 2. The main dimensions are shaft diameter size D_h, impeller inlet diameter D_s, outer diameter size D_2, blade inlet width b_1, front mounting angle Φ_1, rear mounting angle Φ_2, blade wrapping angle $\Delta\varphi$ and so on. The principle of determining the main dimensions is to minimise the flow losses to improve the efficiency of the motor [29].

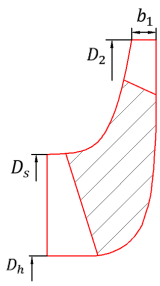

Figure 2. Schematic diagram of the main structure and dimensions of the impeller.

3.2. Number of Leaf Blades

In ventilators, increasing the number of impeller blades increases the theoretical pressure of the impeller because it reduces the effect of relative eddies. However, an increase in the number of blades will increase the friction losses in the impeller channel, which will reduce the actual pressure of the fan and increase energy consumption. Also, the number of blades in a fan cannot be determined theoretically [30]. The fan blades of the scheme before optimisation in this paper were 10.

3.3. Specific Speed

Most of the similarity criterion expressions for impeller machinery contain the characteristic length l, which has some limitations in its use. The specific rotational speed is a similarity criterion consisting of several parameters without the characteristic length. The use of specific rotational speeds can bring much convenience to the design, testing, and classification of impeller machinery [31]. Taking the fan in this paper as an example, the specific rotational speed is as follows:

$$n_s = 5.54n\frac{Q^{\frac{1}{2}}}{\left(\frac{1.2}{\rho}P\right)^{\frac{3}{4}}} = 4.83n\frac{Q^{\frac{1}{2}}}{\left(\frac{P}{\rho}\right)^{\frac{3}{4}}} \tag{3}$$

In this paper, the fan-specific speed n_s is 320. It is known that the fan type is mixed flow.

3.4. Determination of Blade Meridian Surfaces

The meridian curve is a Bezier curve, as shown in Figure 3. The Bezier curve is simple, flexible, has high order continuity and good convexity preservation, and is widely used for the optimal design of the flow within the impeller machinery [32]. The Nth Bezier curve is defined as follows:

$$P(t) = \sum_{i=0}^{n} B_{(i,n)}(t)P_i \;\; 0 \le t \le 1 \tag{4}$$

where $B_{(i,n)}(t)$ is the Bernstein basis function, i.e.,

$$B_{(i,n)}(t) = C_n^i\left(1-t\right)^{n-i}t^i \tag{5}$$

where, P_i is any point on the curve; $t \in (0,1)$ is the covariate. C_n^i is the number of combinations; generally called the fold $P_0P_1P_2\cdots P_n$ is the control polygon of the curve $P(t)$; P_i is the control vertex of the Bezier curve.

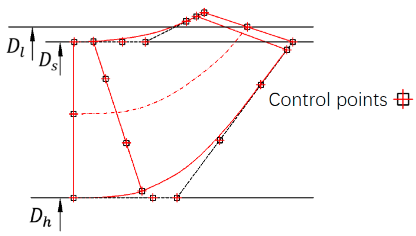

Figure 3. Blade meridian Bezier curve hydrodynamic diagrams.

4. Theory Related to Finite Element Fluid-Structure Coupling Calculations

(1) When the pressure variation through the interior of the motor is small (i.e., a few tens of Pascals), with reference to an isentropic transformation [18], the relative change in density can be calculated from Equation (6):

$$\frac{\Delta\rho}{\rho} = \left[1+\frac{\Delta p}{p}\right]^{\frac{1}{k}} - 1 \tag{6}$$

The flow can be approximated as incompressible and the air density change is negligible.

(2) The standard k-ε model requires solving the equations for turbulent kinetic energy and its dissipation rate. This model assumes that the flow is fully turbulent and that the effect of molecular viscosity can be neglected [33]. The equations for turbulent kinetic energy k and dissipation rate ε for the standard k-ε model are of the following form:

$$\rho\frac{dk}{dt} = \frac{\partial}{\partial x_i}\left[\left(\mu+\frac{\mu_t}{\sigma_k}\right)\frac{\partial k}{\partial x_i}\right] + G_k + G_b - \rho\varepsilon - Y_M \tag{7}$$

$$\rho\frac{d\varepsilon}{dt} = \frac{\partial}{\partial x_i}\left[\left(\mu+\frac{\mu_t}{\sigma_\varepsilon}\right)\frac{\partial \varepsilon}{\partial x_i}\right] + C_{1\varepsilon}\frac{\varepsilon}{k}(G_k + C_{3\varepsilon}G_b) - C_{2\varepsilon}\rho\frac{\varepsilon^2}{k} \tag{8}$$

where G_k denotes the turbulent energy production due to the mean velocity gradient, G_b denotes the turbulent energy production due to the buoyancy effect, and Y_M denotes the effect of the pulsating expansion of the compressible turbulence on the total dissipation rate. The turbulent viscosity coefficient $\mu_t = \rho C_\mu \frac{k^2}{\varepsilon}$. In commercial CFD, the default constants are generally $C_{1\varepsilon} = 1.44, C_{2\varepsilon} = 1.92, C_{3\varepsilon} = 0.09$. The turbulent Platt's numbers for turbulence kinetic energy k and dissipation rate ε are $\sigma_k = 1.0, \sigma_\varepsilon = 1.3$, respectively. In this paper, the standard k-ε turbulence model is used.

(3) The rotation of the motor coaxial fan is the main power source for airflow around the motor. For this strong rotation problem of fluid fields, this paper adopts the rotating coordinate system method (MRF) of computational fluid dynamics software. This method can better simulate the airflow brought about by the fan rotation, and at the same time, it can guarantee a certain calculation accuracy, and the calculation speed is fast, which is suitable for the coupled calculation of the fluid field and temperature field.

5. Inverse Design Motor Fan and Optimisation Analysis

The existing motor fan is reconstructed, and parameters are identified using the RE inverse technique. Then finite element simulation experiments are carried out to analyse the effect of different fan structure parameters on mechanical energy loss. Finally, the fan model that meets the requirements is obtained by correcting the fan parameters through feedback. The specific process is shown in Figure 4.

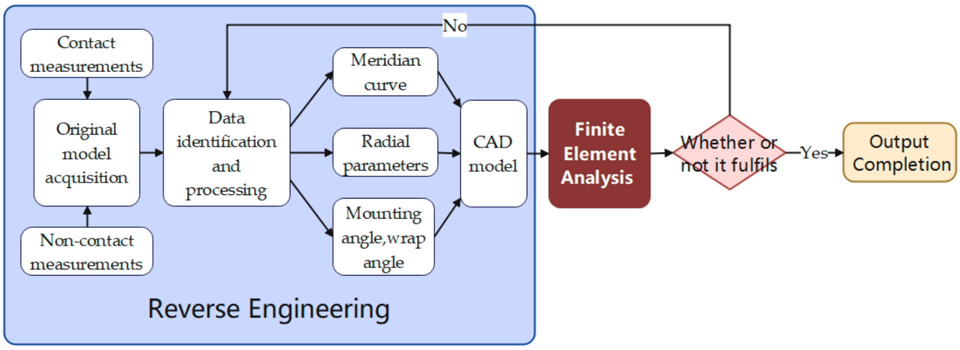

Figure 4. RE design fan process.

5.1. Fan Model Reconstruction

According to the above introduction of the fan as well as the main parameters of the impeller, the existing motor fan model was first reconstructed using RE software (ANSYS-CFturbo 2022), and the parameters were identified.

5.1.1. Inverse Meridian Schematic

Parametric identification of the meridian plane was performed, and the results are shown in Figure 5 below.

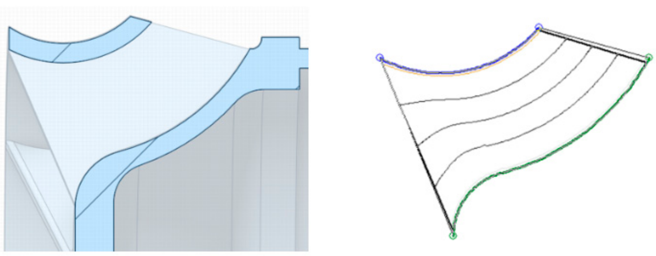

Figure 5. Plot of the original model with inverse capture of the meridian profile.

5.1.2. Fan Radial Main Parameters

The main dimensional parameters are shown in Table 1.

Table 1. Inverse the main radial dimensional parameters of the model.

Parameters	Numerical Value/mm	Schema
D_s	295.3	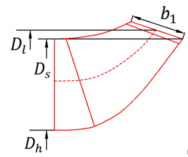
D_l	302.0	
D_h	217.2	
b_2	25.1	

5.1.3. Inverse Model Front and Rear Mounting Angles

Capturing the front and rear mounting angles of the original model can be used to build a new model with different combinations of front and rear mounting angles. The front and rear mounting angles are shown in Figure 6, and the original model has 90° front and rear mounting angles.

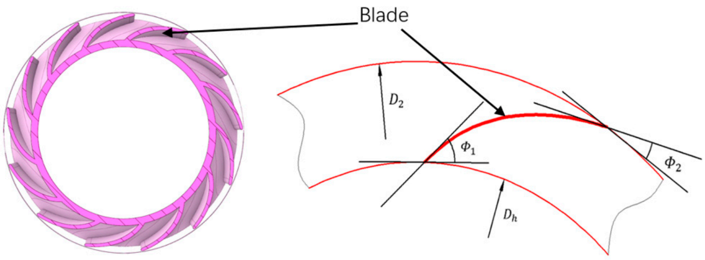

Front mounting angle Φ_1/(°)	Rear mounting angle Φ_2/(°)
$0 \le \Phi_1 \le 90°$	$0 \le \Phi_2 \le 90°$

Figure 6. Schematic diagram of front and rear mounting angles and range of values.

5.1.4. Impeller Wrap Angle Parameter

The fan impeller structure corresponding to different wrap angles Δφ is shown in Figure 7, and the original fan model has a wrap angle of 0°.

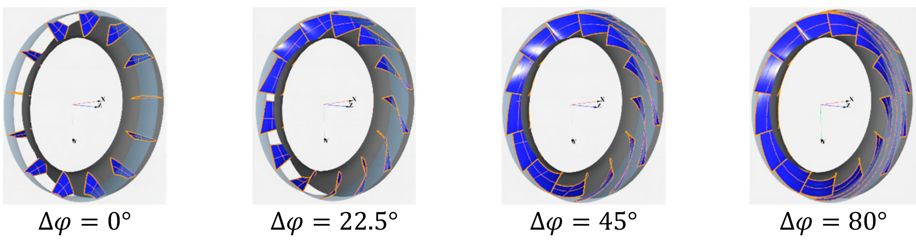

Figure 7. Schematic diagrams of fan impellers with different wrap angles.

5.1.5. Optimisation of Impeller Rim Edge

As shown in Figure 8, the leading edge and trailing edge of the impeller are chamfered with Bezier curves instead of right angles in the original model.

(**a**) (**b**)

Figure 8. Schematic before and after optimisation of leading and trailing edges. (**a**) Original model impeller rim edge; (**b**) Optimised model impeller edge.

5.2. Simulation Analysis and Optimisation of Fan External Flow Field

To analyse and optimise the performance of the fan, the main research method is to use CFD software to carry out finite element analysis on different parameters of the fan, and to study the effect of the structural parameters of the fan on its aerodynamic performance. The external flow field of the fan is created as shown in Figure 9, and the CFD hydrodynamic analysis of the fan is carried out in the external flow field to determine the mechanical energy loss and fan resistance according to the simulation results and further to determine the optimal fan structure, so as to complete the optimisation and improvement of the fan impeller.

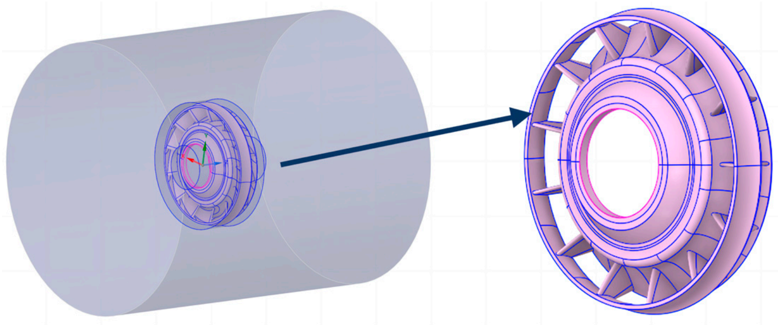

Figure 9. Simulation models of outflow fields.

This paper focuses on the simulation analysis of the fan with different wrap angles $\Delta\varphi$ and number of blades Z to achieve a reduction in the energy consumption of the fan based on the flow rate of the new fan being greater than or equal to that of the prototype fan. Therefore, compared to conventional fan optimisation, which is more concerned with full pressure efficiency or static pressure efficiency, this paper focuses on the ability of the fan to generate airflow and the magnitude of mechanical energy loss. The efficiency evaluation index of the fan [34] is calculated as follows:

$$\eta = \frac{P_v \times Q_v}{M \times w} \tag{9}$$

where P_v is the outlet dynamic pressure, Q_v is the volume of gas flowing in and out of the flow field per unit time, M is the torque supplied to the fan by the shaft, and w is the fan speed.

Considering the complexity of the computational model and the time period of the finite element computation of the flow and temperature fields, this paper is mainly based on the optimisation method of the univariate function. The univariate function optimisation design is carried out for the fan's wrap angle and the blades, as the change of the fan's wrap angle and the blades often results in an optimised design with greater benefits.

The simulation analysis of the external flow field was done for the fan wrap angles $\Delta\varphi$ of 0°, 30°, 60° and 85°, respectively, as shown in Figure 10a–d. The velocity trace, velocity cloud, ZY-plane pressure cloud, and XY-plane pressure cloud are shown in the figures, respectively.

From the above simulation cloud results, it can be seen that the velocity traces of the outflow field have a significant difference as the wrap angle changes. At the same time, with the maximum speed of the fan, the blade pressure also changes. From the results, the corresponding outlet dynamic pressure P_v, flow volume Q_v, and fan torque M can be extracted, which in turn leads to the fan efficiency evaluation index η under different wrap angles as shown in Figure 11. It can be seen that when the wrap angle $\Delta\varphi$ = 60°, the fan efficiency evaluation index $\eta = 0.28$ is the optimal value.

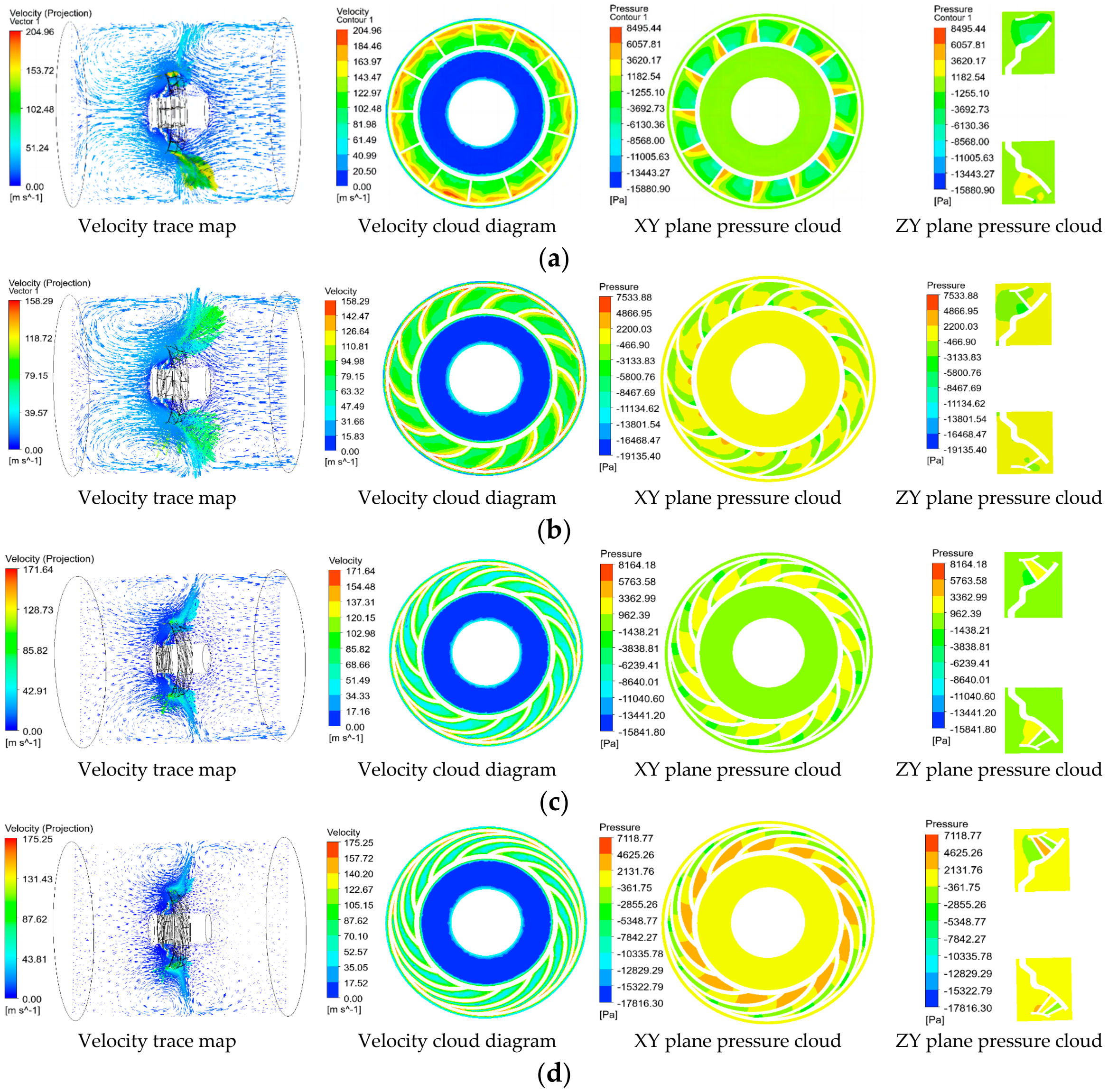

Figure 10. Comparison of simulation results of fan external flow field under different wrap angles. (**a**) $\Delta\varphi = 0°$, Z = 13; (**b**) $\Delta\varphi = 30°$, Z = 13; (**c**) $\Delta\varphi = 60°$, Z = 13; (**d**) $\Delta\varphi = 85°$, Z = 13.

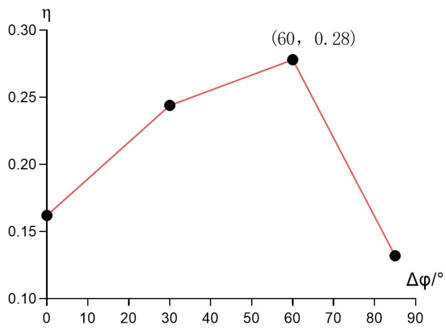

Figure 11. Evaluation indexes of fan efficiency η corresponding to different wrap angles Δφ.

From the above simulation cloud results, it can be seen that the velocity traces of the outflow field have a significant difference as the wrap angle changes. At the same time, with the maximum speed of the fan, the blade pressure also changes. Under different package angles, the corresponding outlet dynamic pressure P_v, flow volume Q_v, fan torque M and other data can be extracted from the simulation results of the fan. And then, according to

Equation (9), calculate the fan efficiency evaluation index η under different wrap angle, and the results are shown in Figure 11. It can be seen that when the wrap angle $\Delta\varphi$ = 60°, the fan efficiency evaluation index $\eta = 0.28$ is the optimal value.

Similarly, the finite element simulation analysis of the external flow field of the fan corresponding to different numbers of blades is carried out, and the results are shown in Figure 12.

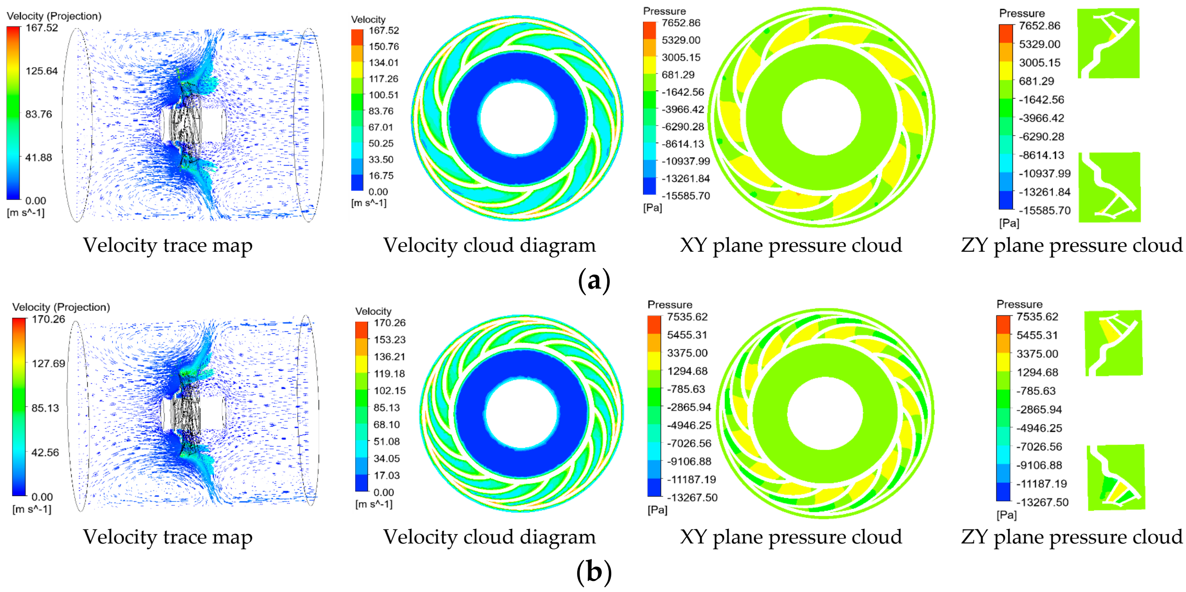

Figure 12. Comparison of simulation results of fan outflow field under different blade numbers. (**a**) $\Delta\varphi = 60°$, Z = 10; (**b**) $\Delta\varphi = 60°$, Z = 15.

For different numbers of blades, the corresponding outlet dynamic pressure P_v, flow volume Q_v, fan torque M and other data can be extracted from the simulation results of the fan. According to Equation (9), the fan efficiency evaluation index η is calculated under different blades, and the results are shown in Figure 13. It can be seen that when blade Z = 13, the fan efficiency evaluation index η = 0.28 is the optimal value.

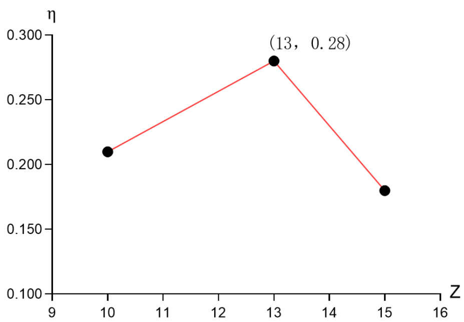

Figure 13. Fan efficiency evaluation index η optimal point.

Finally, combining Figures 11 and 13, it can be seen that the fan efficiency evaluation index is optimal when $\Delta\varphi$ =60° and Z = 13.

5.3. Comparative Simulation Analysis of Motor Temperature Field

Based on the fan optimisation model derived from Section 5.2, the effect of the pre-optimisation and post-optimisation fan models on the temperature field of the motor is analysed. Table 2 shows the comparison of the relevant parameters of the motor fan before and after optimisation.

Table 2. Comparison of motor fan parameters before and after optimisation.

Item	Edge	Wrap Angle $\Delta\varphi/(^\circ)$	Blade Number Z	Front Mounting Angle $\Phi_1/(^\circ)$	Rear Mounting Angle $\Phi_2/(^\circ)$	3D Model
Before optimisation	Right angle	0	10	90	90	
After optimisation	Bezier's angle	60	13	45	30	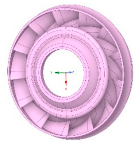

In the thermal simulation analysis of the motor, the losses of each component of the motor are first calculated at 9000 rev/min operating conditions. In this paper, the electromagnetic loss of the motor is obtained by simulation calculation through the finite element method, and then the heat generation rate of each component in the motor is obtained according to the volume of each component [35]. The heat generation rate of each component is shown in Table 3.

Table 3. Heat generation rate of motor components.

Components	Loss (W)	Volumes (m^3)	Heat Generation Rate (W/m^3)
Winding copper consumption	5080	0.0098	518,367.3
Stator iron consumption	2630	0.0098	268,367.3
Rotor iron consumption	486	0.0068	71,470.6
Magnets	1000	0.0021	476,190.5

In the coupled simulation of the temperature field and flow field of the motor, certain boundary conditions are imposed on the simulation model according to the structure of the motor and the actual working environment. Mass flow boundary conditions are applied to the cooling water inlet, and pressure outlet boundary conditions are applied to the outlet. The boundary conditions imposed during the finite element analysis are shown in Table 4. The heat generation rate from Table 5 is applied as a heat source loaded on each heat-generating part on average.

Table 4. Calculation of boundary conditions.

Position	Boundary Conditions	Value
Water inlet	Velocity inlet	2.04 m/s, 70 °C
Water outlet	Pressure outlet	1 Pa
Outer wall surface of housing	Natural Convection heat Dissipation	10 W/($m^2 \cdot K$), 70 °C
Rotating part	Field of rotation	9000 rev/min
Water jacket and stator OD contact surface	Coupling surface	0.5 mm, 0.21 W/($m \cdot K$)

Table 5. Comparison of motor performance.

	Maximum Magnet Temperature T_{max}/(°C)	Maximum Winding Temperature T_{cu}/(°C)	Maximum Temperature Rise ΔT/(K)	Mechanical Energy Loss P_{mech}/(kW)	Efficiency η_0
Before optimisation	205.4	168.5	135.4	8.0	94.2%
After optimisation	188.7	158.3	118.7	2.54	96.1%

According to the finite element software calculation and solution, a comparison of the pre-optimisation and post-optimisation motor temperature field results is shown in Figure 14. The temperature cloud data of the magnet, rotor core, windings, and XY plane can be known. Comparing the temperature cloud data of each component, it can be obtained:

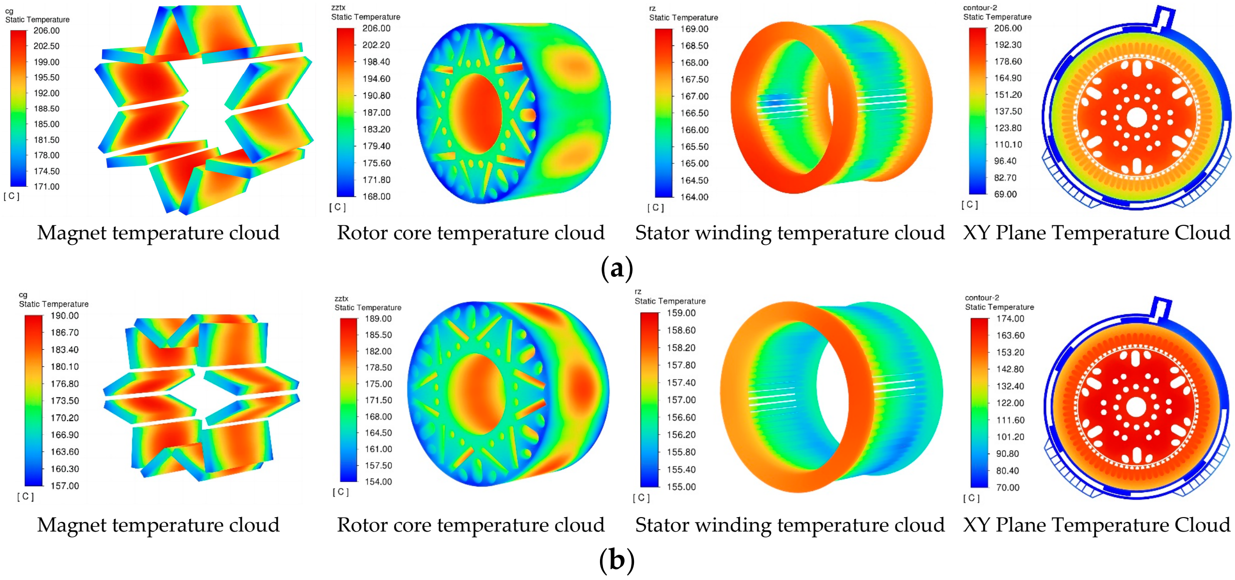

Figure 14. Comparison of motor temperature field results for two fan schemes. (**a**) Optimisation of the previous fan solution; (**b**) Optimised fan solution.

(1) The results before optimisation are shown in Figure 14a. By extracting the finite element simulation to calculate the temperature data of each component, it can be seen that the maximum temperature of the motor is 205.4 °C at the magnet position. The calculation by extracting the finite element simulation data shows that the fan torque after optimisation is 8.4 Nm. According to Equation (2), the mechanical energy loss is P_{mech} =8.0 kW.

(2) The optimised results are shown in Figure 14b. By extracting the finite element simulation to calculate the temperature data of each component, it can be seen that the highest temperature of the motor is 188.7 °C at the magnet position. The calculation by extracting the finite element simulation data shows that the optimised fan torque is 2.7 Nm. According to Equation (2), the mechanical energy loss is P_{mech} =2.54 kW.

As shown in Table 5, it can be seen that the maximum temperature T_{max} of the motor decreases by 16.7 K, the electromagnetic performance of the motor is greatly improved, the mechanical energy loss decreases by 5.46 kW, and the efficiency of the motor is improved by 1.9%.

After optimising the design, the main dimensional parameters of the motor as well as the fan are shown in Table 6.

Table 6. Main structural parameters of motor and fan.

Motor Main Structure Parameters		Main Structural Parameters of Fan	
Parameter	**Value**	**Parameter**	**Value**
Rated power (kW)	350	shaft diameter size (mm)	217.2
Rated speed (r/min)	9000	impeller inlet diameter (mm)	295.3
Stator outer diameter (mm)	450	outer diameter size (mm)	302
Stator inner diameter (mm)	320	Wrap angle (°)	60
Rotor outer diameter (mm)	314	Blade number	13
Iron core length (mm)	180	Front mounting angle (°)	45
Number of pole pairs	3	Rear mounting angle (°)	30

6. Conclusions

In this paper, a parametric identification of the axis fan of a special motor is carried out by applying Reverse Engineering (RE). Computational fluid dynamics methods are used to analyse the effects of several geometrical parameters on the dynamic performance of the fan blades. Simulation analysis is carried out for the fan parameters, and an optimisation scheme is proposed to achieve an improvement in the performance of the motor fan. Further finite element simulation comparison experiments are carried out on the motor fan before and after optimisation. The final results show that, compared with the pre-optimisation scheme, the maximum temperature of the motor decreases by 16.7 K, the mechanical energy loss decreases significantly, and the motor efficiency increases by 1.9%. The following main conclusions are drawn from the optimisation analysis of several fan parameters and the simulation calculation of the motor temperature field:

(1) Using the inverse solution technique, the fan can be accurately modelled with parameter identification to improve the speed and accuracy of motor fan design calculations.

(2) The wrap angle of the motor axis fan has a large impact on the fan performance, and there is an optimal wrap angle, which makes the motor axis fan have the highest efficiency and the smallest mechanical energy loss, greatly reduces the temperature rise of the motor, and improves the overall performance of the motor.

(3) A more accurate finite element calculation method for the mechanical loss of the enclosed motor axis fan is proposed.

Author Contributions: Conceptualization, C.M.; Methodology, C.M.; Software, Z.H.; Validation, Z.H.; Formal analysis, C.L.; Investigation, C.L. and D.P.; Resources, K.L. and D.P.; Data curation, K.L.; Writing—original draft, C.M. and W.H.; Writing—review & editing, W.H.; Supervision, C.L.; Project administration, C.L. and W.H.; Funding acquisition, W.H. All authors have read and agreed to the published version of the manuscript.

Funding: This research received no external funding.

Conflicts of Interest: The authors declare no conflict of interest.

References

1. Woo, J.-H.; Lee, J.-K.; Choi, J.; Kim, H.; Lee, J. Design of V-type IPMSM for a military vehicle which takes consideration of the output characteristic on the high speed. In Proceedings of the 2016 19th International Conference on Electrical Machines and Systems (ICEMS), Chiba, Japan, 13–16 November 2016; pp. 1–4.
2. Espanet, C.; Kauffmann, J.-M.; Bernard, R. Comparison of Two In-Wheel Permanent Magnet Motors for Military Applications. In Proceedings of the 2006 IEEE Vehicle Power and Propulsion Conference, Windsor, UK, 6–8 September 2006; IEEE: Piscataway, NJ, USA, 2006; pp. 1–6.
3. Li, W.; Cao, Z.; Zhang, X. Thermal Analysis of the Solid Rotor Permanent Magnet Synchronous Motors with Air-Cooled Hybrid Ventilation Systems. *IEEE Trans. Ind. Electron.* **2022**, *69*, 1146–1156. [CrossRef]
4. Liu, F.; Wang, X.; Xing, Z.; Ren, J.; Li, X. Analysis and Research on No-Load Air Gap Magnetic Field and System Multiobjective Optimization of Interior PM Motor. *IEEE Trans. Ind. Electron.* **2022**, *69*, 10915–10925. [CrossRef]

5. Jiang, W.; Jahns, T.M. Coupled Electromagnetic–Thermal Analysis of Electric Machines Including Transient Operation Based on Finite-Element Techniques. *IEEE Trans. Ind. Appl.* **2015**, *51*, 1880–1889. [CrossRef]
6. Li, J.; Gao, J.; He, Z.; Huang, S.; Hu, C.; Wu, Y. Analysis of Fluid Field and Temperature Field of Permanent Magnet Synchronous Motor for Special Vehicles. In Proceedings of the 2023 2nd International Conference on Mechatronics and Electrical Engineering (MEEE), Abu Dhabi, United Arab Emirates, 10–12 February 2023; IEEE: Piscataway, NJ, USA, 2023; pp. 1–5.
7. Sciascera, C.; Giangrande, P.; Papini, L.; Gerada, C.; Galea, M. Analytical Thermal Model for Fast Stator Winding Temperature Prediction. *IEEE Trans. Ind. Electron.* **2017**, *64*, 6116–6126. [CrossRef]
8. Mellor, P.H.; Yon, J.; Baker, J.L.; North, D.; Booker, J.D. Electromagnetic and thermal coupling within a fault-tolerant aircraft propulsion motor. In Proceedings of the IEEE International Electric Machines and Drives Conference, Miami, FL, USA, 21–24 May 2017; pp. 1–7.
9. Bonnett, H. Operating temperature considerations and performance characteristics for IEEE 841 motors. *IEEE Trans. Ind. Appl.* **2001**, *37*, 1120–1131. [CrossRef]
10. Albers, T.; Bonnett, A.H. Motor temperature considerations for pulp and paper mill applications. *IEEE Trans. Ind. Appl.* **2002**, *38*, 1701–1713. [CrossRef]
11. Bellettre, J.; Sartre, V.; Biais, F.; Lallemand, A. Transient state study of electric motor heating and phase change solid-liquid cooling. *Appl. Thermal Eng.* **1997**, *17*, 17–31. [CrossRef]
12. Sun, Z. Design and Temperature Rise Calculation of Permanent Magnet Propulsion Motor for 350kW Tank. Master's Thesis, Shenyang University of Technology, Shenyang, China, 2018.
13. Gai, Y.; Kimiabeigi, M.; Chuan Chong, Y.; Widmer, J.D.; Deng, X.; Popescu, M.; Goss, J.; Staton, D.A.; Steven, A. Cooling of Automotive Traction Motors: Schemes, Examples, and Computation Methods. *IEEE Trans. Ind. Electron.* **2019**, *66*, 1681–1692. [CrossRef]
14. Huang, J.; Shoai Naini, S.; Miller, R.; Rizzo, D.; Sebeck, K.; Shurin, S.; Wagner, J. A Hybrid Electric Vehicle Motor Cooling System—Design, Model, and Control. *IEEE Trans. Veh. Technol.* **2019**, *68*, 4467–4478. [CrossRef]
15. Li, H. Cooling of a permanent magnet electric motor with a centrifugal impeller. *Int. J. Heat Mass Transf.* **2010**, *53*, 797–810. [CrossRef]
16. Kim, C.; Lee, K.-S.; Yook, S.-J. Effect of air-gap fans on cooling of windings in a large-capacity, high-speed induction motor. *Appl. Therm. Eng.* **2016**, *100*, 658–667. [CrossRef]
17. Gebauer, M.; Blejchař, T.; Brzobohatý, T.; Karásek, T.; Nevřela, M. Determination of Aerodynamic Losses of Electric Motors. *Symmetry* **2022**, *14*, 2399. [CrossRef]
18. Galloni, E.; Parisi, P.; Marignetti, F.; Volpe, G. CFD analyses of a radial fan for electric motor cooling. *Therm. Sci. Eng. Prog.* **2018**, *8*, 470–476. [CrossRef]
19. Nakahama, T.; Biswas, D.; Kawano, K.; Ishibashi, F. Improved Cooling Performance of Large Motors Using Fans. *IEEE Trans. Energy Convers.* **2006**, *21*, 324–331. [CrossRef]
20. Lee, K.-H.; Cha, H.-R.; Kim, Y.-B. Development of an interior permanent magnet motor through rotor cooling for electric vehicles. *Appl. Therm. Eng.* **2016**, *95*, 348–356. [CrossRef]
21. Nakahama, T.; Suzuki, K.; Hashidume, S.; Ishibashi, F.; Hirata, M. Cooling Airflow in Unidirectional Ventilated Open-Type Motor for Electric Vehicles. *IEEE Trans. Energy Convers.* **2006**, *21*, 645–651. [CrossRef]
22. Shao, Y.F. Inverse Design and Performance Analysis of a High-Speed Motor Fan Structure. Master's Thesis, Shenyang University of Technology, Shenyang, China, 2021.
23. Wang, J.Q. Research on Reverse Design and Key Technology Based on Curved Surface of Unpowered Exhaust Fan Blade. Master's Thesis, North University of Technology, Beijing, China, 2009.
24. Gong, C. Research and Modification Design of Automotive Cooling Fan Blade Based on Reverse Engineering. Master's Thesis, Yanshan University, Qinhuangdao, China, 2012.
25. Jim, C. Reverse Modelling and Optimal Design of Automotive Engine Blade. Master's Thesis, Nanjing University of Aeronautics and Astronautics, Nanjing, China, 2009.
26. Liu, F.; Li, Z.; Huang, J. Consideration of a new fan structure for an ultra-high efficiency motor. *Electr. Mach. Control Appl.* **2010**, *37*, 18–20.
27. Chapman, S.J. *Electirc Machinery Fundamentals*; Publishing House of Electronics Industry: Beijing, China, 2014.
28. Zaher, I.; Rodriguez, R.; Sayed, E.; Callegaro, A.; Goykhman, M.; Emadi, A. Effect of Rotor Geometry on Rotor Air Cooling of a Ventilated Axial-Flux Permanent Magnet Machine. In Proceedings of the 2021 IEEE Transportation Electrification Conference & Expo (ITEC), Chicago, IL, USA, 21–25 June 2021; IEEE: Piscataway, NJ, USA, 2021; pp. 77–82.
29. Shang, J. *Handbook of Practical Technology of Ventilators*; China Machine Press: Beijing, China, 2011.
30. Eck, B. *Fans: Design and Operation of Centrifugal, Axial-Flow, and Cross-Flow Fans*; Pergamon Press: Berlin, Germany, 1973.
31. Cheng, X. *Vane Pump-Ventilator-Compressor (Principle, Design, Operation, Strength)*; China Machine Press: Beijing, China, 2011.
32. Li, Y.; Chen, D.; Dai, L. Preferred design of radial turbine blade radial surface profile. *J. Eng. Thermophys.* **2013**, *34*, 853–857.
33. Zhang, D.S.; Zhang, Q.H.; Shi, W.D. *Fundamentals and Applications of Numerical Simulation for Vane Pump Design*; China Machine Press: Beijing, China, 2015.

34. Rui, Z. Simulation and Optimisation of Fan and Impeller Field Based on CFD. Master's Thesis, Southeast University, Nanjing, China, 2016.
35. Pyrhönen, J.; Jokinen, T.; Hrabovcová, V. *Design of Rotating Electrical Machines*; China Machine Press: Beijing, China, 2018.